



Effect of heat treatment temperature on the morphology and upconversion properties of LaF₃:Yb,Er nanoparticles

Borbála Tegze¹ · Gyula Tolnai² · Dóra Hessz^{1,3} · Miklós Kubinyi¹ · János Madarász⁴ · György Sáfrán⁵ · Zoltán Hórvölgyi¹

Received: 28 June 2023 / Accepted: 17 July 2023 / Published online: 4 August 2023
© The Author(s) 2023

Abstract

LaF₃:5%Yb³⁺,0.5%Er³⁺ upconverting nanoparticles were synthesized with co-precipitation method and heat treated at temperatures 300–600 °C. The morphology of the particles was characterized by high-resolution transmission electron microscopy coupled with energy-dispersive spectrometry and dynamic light scattering. Crystal structure was studied by X-ray diffraction (XRD), and thermal behaviour was investigated by simultaneous thermogravimetry and differential thermal analysis (TG/DTA). Upconversion behaviour was studied in detail by fluorescence spectroscopy, with 980 nm excitation. Particle sizes increased with increasing heat treatment temperature, and samples showed significant aggregation above 500 °C. Hexagonal LaF₃ crystal structure was identified for all samples, with increased crystallinity after heat treatment at 400 °C, which was corroborated with TG/DTA results. XRD and energy-dispersive spectrometry results revealed that at higher temperatures new crystal phases formed, as some Yb³⁺ and Er³⁺ dopant ions segregated into new nanocrystals, made of, *for example*, YbOF and YbOOH, which caused a significant decrease in the upconversion emission of the samples. The highest upconversion emission was achieved after heat treatment at 400 °C.

Keywords Upconversion · Nanoparticles · Heat treatment · Thermal analysis · Lanthanide · Co-precipitation

Introduction

Upconverting nanoparticles (UCNPs) are recently attracting growing interest, due to their promising applications in the fields of biomedicine and bioanalysis [1, 2], photocatalysis and photovoltaics [3, 4], sensors and optoelectronic devices [5, 6], security applications [7], etc. During the upconversion

process, the material absorbs multiple photons of lower energy (typically in the near infrared range) and then emits a photon of higher energy (in the visible or ultraviolet range). UCNPs are mainly rare earth (RE)-doped materials, consisting of a host lattice and several doping ions [8, 9]. The most promising host materials are fluoride materials, prominently LaF₃ and NaYF₄. LaF₃ has many advantages, such as low vibrational energy, good stability and close lattice match to the dopant RE ions; furthermore, they have generally simpler synthesis routes compared to NaYF₄ nanoparticles [8, 10]. The doping ions are RE ions, and the most often used are Yb³⁺, Er³⁺ and Tm³⁺; the host material is typically co-doped with a sensitizer ion, which has good absorption properties (*e.g.* Yb³⁺ which absorbs 980 nm near infrared light) and able to transfer energy to the other doping ion, called the activator ion (*e.g.* Er³⁺ and Tm³⁺), which determines the emission spectrum of the system [8, 9].

RE-doped LaF₃ nanoparticles can be synthesized by different synthesis methods, including thermal decomposition, solvothermal synthesis and co-precipitation. Co-precipitation is a relatively low-cost and simple method, without the need of complex equipment or harsh reaction conditions, *i.e.*

✉ Zoltán Hórvölgyi
horvolgyi.zoltan@vbk.bme.hu

¹ Department of Physical Chemistry and Materials Science, Budapest University of Technology and Economics, H-1111, Műegyetem Rkp. 3., Budapest, Hungary

² Holikem Kft, H-1082, Kisfaludy Utca 40, Budapest, Hungary

³ MTA-BME Lendület Quantum Chemistry Research Group, Műegyetem Rkp. 3., H-1111, Budapest, Hungary

⁴ Department of Inorganic and Analytical Chemistry, Budapest University of Technology and Economics, H-1111, Műegyetem Rkp. 3., Budapest, Hungary

⁵ Thin Film Physics Department, Centre for Energy Research, Institute of Technical Physics and Materials Science, H-1121, Konkoly-Thege M. Street 29-33, Budapest, Hungary

high temperatures, while it is able to provide small particles with a narrow size distribution [9, 11]. However, usually post-synthesis heat treatments are needed to attain suitable upconversion properties. Previous studies show that heat treatment plays a very important role in the achieved upconversion properties of UCNPs prepared by co-precipitation [12, 13], including RE-doped LaF₃ particles [14–16]. Poma et al. [14] studied LaF₃/20%Yb,5%Er particles synthesized by aqueous co-precipitation and heat treated at 300–900 °C and found that the UCNPs only showed measurable upconversion emission after treatment at and above 500 °C, which they attributed to low crystallinity, higher amount of surface defects and possible impurities present in the particles made without heat treatment or at lower temperatures. Shen et al. [15] similarly prepared LaF₃/20%Yb,5%Er particles by co-precipitation and post-treatment at 180–600 °C: according to their results, higher heat treatment temperatures lead to higher emissions, with the samples heat treated at 600 °C showing the best upconversion properties, which they explained with the higher crystallinity and particles sizes. Acosta et al. [16] synthesized LaF₃/12–20%Yb,3–5%Er particles by co-precipitation, followed by heat treatment at 400–600 °C, and they also found that upconversion emission increased with increasing heat treatment.

These results show that investigating the effect of heat treatment is very important; however, in these studies the optimum temperature of the heat treatment is not clearly found, and more detailed investigations would be beneficial. Furthermore, all above studies were carried out on LaF₃/Yb,Er particles with similar, relatively high doping ion concentration (above 10 mol% for Yb³⁺, and above 3 mol% for Er³⁺), and it is worth noting that doping ion concentration can also influence how the upconversion properties depend on the heat treatment [13]. UCNPs with much lower doping ion concentration can be interesting for many practical applications, as they can still show suitable upconversion properties, while necessitating less RE material for their synthesis, which can significantly lower the cost of a product. In this paper, our aim is to investigate the role of the heat treatment in the properties of RE-doped LaF₃ nanocrystals with relatively low doping ion concentrations (LaF₃/5 mol% Yb³⁺, 0.5 mol% Er³⁺), and find an optimal heat treatment temperature. The aim is to prepare UCNPs with the highest possible upconversion emission, while also keeping in mind that for many applications small particle sizes and narrow size distribution should be prioritized. UCNPs were synthesized by co-precipitation method and heat treated at temperatures 300–600 °C. The morphology of the particles was characterized by high-resolution transmission electron microscopy coupled with energy-dispersive spectrometry, and dynamic light scattering. Crystal structure was studied by X-ray diffraction analysis, and thermal behaviour was investigated by simultaneous thermogravimetry and

differential thermal analysis. Upconversion behaviour was studied in detail by fluorescence spectroscopy, using 980 nm laser light source for excitation.

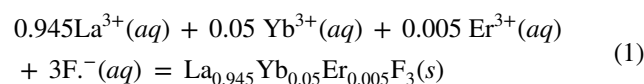
Experimental

Materials

Lanthanum oxide (La₂O₃, 99.9%), ytterbium oxide (Yb₂O₃, 99.9%), erbium oxide (Er₂O₃, 99.9%) and sodium fluoride (NaF, 99.99%) were obtained from Alfa Aesar and were of REO grade. Rare earth chloride solutions were prepared by dissolving the corresponding oxides in hydrochloric acid at an elevated temperature and diluted with distilled water. Absolute ethanol (EtOH, 99.7 + %, a.r.) was obtained from Reanal (Budapest, Hungary).

Preparation of upconverting nanoparticles

Nanocrystals of LaF₃ doped with 5 mol% Yb³⁺ ions and 0.5 mol% Er³⁺ ions were synthesized by a precipitation of rare earth chlorides with sodium fluoride. In first step, 96.5 mL La³⁺ solution (100 mM), 10.2 mL Yb³⁺ solution (50 mM) and 1.02 mL Er³⁺ solution (50 mM) were combined and stirred for 30 min and then transferred into a glass reactor (250 mL) equipped with magnetic stirrer and reflux condenser. Separately, 1.5418 g (36.72 mmol) NaF was dissolved in 48 mL of distilled water and preheated to 80 °C. The rare earth chloride solution was heated to 80 °C, and NaF solution was added at precisely controlled speed (1 mL min⁻¹). The temperature of the reaction mixture was kept at 80 °C and stirred for 4 h at 80 °C. Reaction time and temperature were selected based on the work of Sevonkaev et al. [17]. The reaction equation is presented in Eq. (1).



After cooling down to room temperature, the product was collected by centrifugation, washed with distilled water several times, and dried at 80 °C for 24 h in air. Finally, the dried material was powdered. (Average reaction yield was 92%.) To study the effects of heat treatment conditions on the properties of nanocrystals, the as-prepared material was annealed for 2 h at different temperatures (300 °C, 400 °C, 500 °C and 600 °C) in an electric furnace (Nabertherm B170) and collected for characterization. For some characterization methods, the particles were dispersed in ethanol via ultrasonication: ethanol was chosen as medium, since upconverting particles show long-term stability in ethanolic

dispersions, while partial dissolution may occur in aqueous medium after longer storage times [18].

Characterization

The morphology of the nanoparticles was characterized by high-resolution transmission electron microscopy (*TEM/HRTEM/HAADF*), using a JEOL 3010 instrument operated at 300 kV with a point resolution of 0.17 nm. Morphology of the nanocrystals was investigated by transmission electron microscopy (TEM) in HRTEM and scanning TEM (STEM) high-angle annular dark-field (HAADF) modes by means of a FEI Titan Themis 200 kV spherical aberration (Cs)—corrected TEM with 0.09 nm HRTEM and 0.16 nm STEM resolution. Composition of the samples was measured by STEM-EDS (energy-dispersive spectrometry), and elemental maps were obtained by spectrum imaging with 4 Thermo Fisher “Super X G1” EDS detectors built in the microscope. During the sample preparation, 1 mg mL⁻¹ ethanolic suspensions of the nanoparticles were prepared and dispersed by ultrasonication, and then, a droplet of the suspension was deposited onto a carbon-coated copper grid, followed by a drying step under an infrared heat lamp. The average diameters were determined by averaging the values measured on 200–300 individual particles, with the exception of the sample treated at 600 °C, in which case the increased particle sizes and limited number of TEM images taken only allowed for the measurement of ~ 100 particles.

The mean hydrodynamic sizes of the nanoparticles in ethanolic media were characterized by dynamic light scattering (DLS) measurements, using a Zetasizer Nano ZS (Malvern Instruments), with a 532 nm He–Ne laser. 1 mg mL⁻¹ ethanolic suspensions of the nanoparticles was prepared and ultrasonicated for 2 × 15 min prior to the start of the measurement. Z-average mean diameter and polydispersity index values of the particles were determined.

Crystallinity of the samples was characterized by X-ray diffractometer (Philips PANalytical X’pert Pro, with Cu–K α radiation). Measurements were carried out in the 2 θ = 4–84° range, with scanning rate of 5 s/step and step size of 0.0167°. Average crystallite sizes were determined from the highest intensity peak of the XRD pattern (2 θ = 27.8°, corresponding to (111) plane), using Scherrer’s equation [19].

Thermal properties of the nanoparticles were analysed by simultaneous thermogravimetry and differential thermal analysis (TG/DTA). The as-prepared sample was measured in air (130 mL min⁻¹ air flow) by a STD 2960 Simultaneous TG/DTA device; the temperature was changed from room temperature up to 800 °C, with 10 °C min⁻¹ rate of heating.

Upconversion emission was studied by fluorescence spectroscopy (Edinburgh Instruments Spectrofluorometer FS5), using a 980 nm monochromatic laser light source for excitation. The emission spectra of 1 mg mL⁻¹ ethanolic

suspensions of the UCNPs were measured in a quartz cuvette kept at 20.0 °C, between 300 and 700 nm, with a 1 nm step size, 0.5 s dwell time, 1 nm scan slit, and laser power of 1.49 W. The suspensions were ultrasonicated for 2 × 15 min prior to the start of the measurement. Laser power-dependent emission intensity was also measured in the 500–600 nm emission wavelength range on 0.2 mg mL⁻¹ ethanolic suspensions, with laser power changing between 0.28 and 1.18 W, 1 nm step size, 0.5 s dwell time and 5 nm scan slit, at 20.0 °C constant temperature.

Results and discussion

Characterization of morphology, crystal structure and thermal behaviour

Figure 1 shows the TEM images of the samples. Table 1 shows the average particle sizes, while the size distribution diagrams can be seen in Fig. 2. The results show that as the

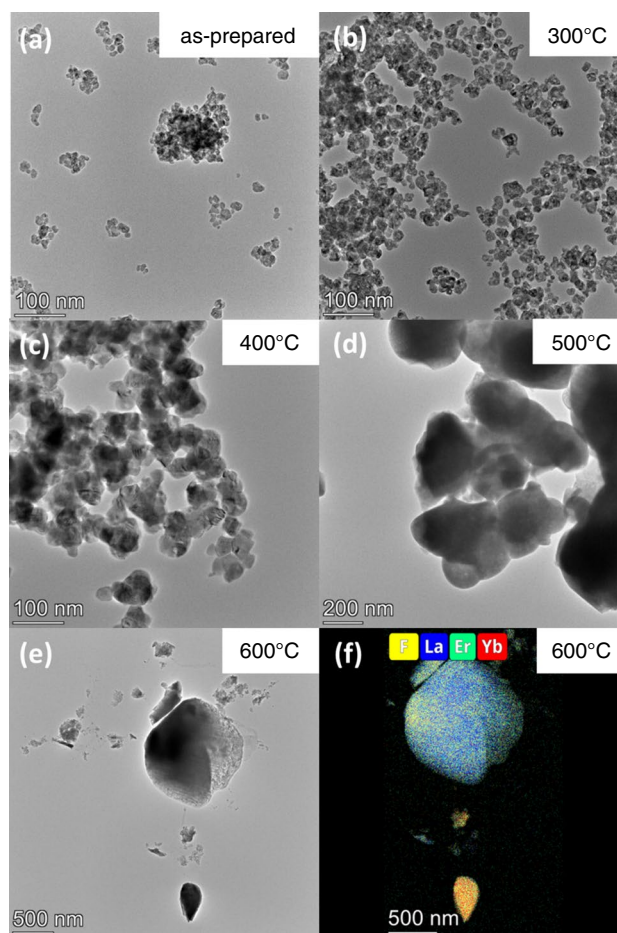


Fig. 1 TEM images of **a** as-prepared, **b–e** heat-treated samples at the indicated temperatures and **f** STEM EDS elemental map of the area in **e** of the heat-treated sample at 600 °C

Table 1 Average particle sizes determined from TEM images

Sample	Average diameter determined by TEM /nm	Average crystallite size determined by XRD /nm	Average hydrodynamic diameter determined by DLS /nm	Polydispersity index determined by DLS
as-prepared	11 ± 3	13.7	201 ± 22	0.255
300 °C	14 ± 4	13.7	196 ± 30	0.251
400 °C	34 ± 9	24.3	133 ± 22	0.226
500 °C	282 ± 132	31.1	1122 ± 32	0.350
600 °C	660 ± 550	68.1	885 ± 30	0.603

Average crystallite sizes determined by XRD from the highest intensity (111) plane peak

Average hydrodynamic diameter and polydispersity index values determined by DLS

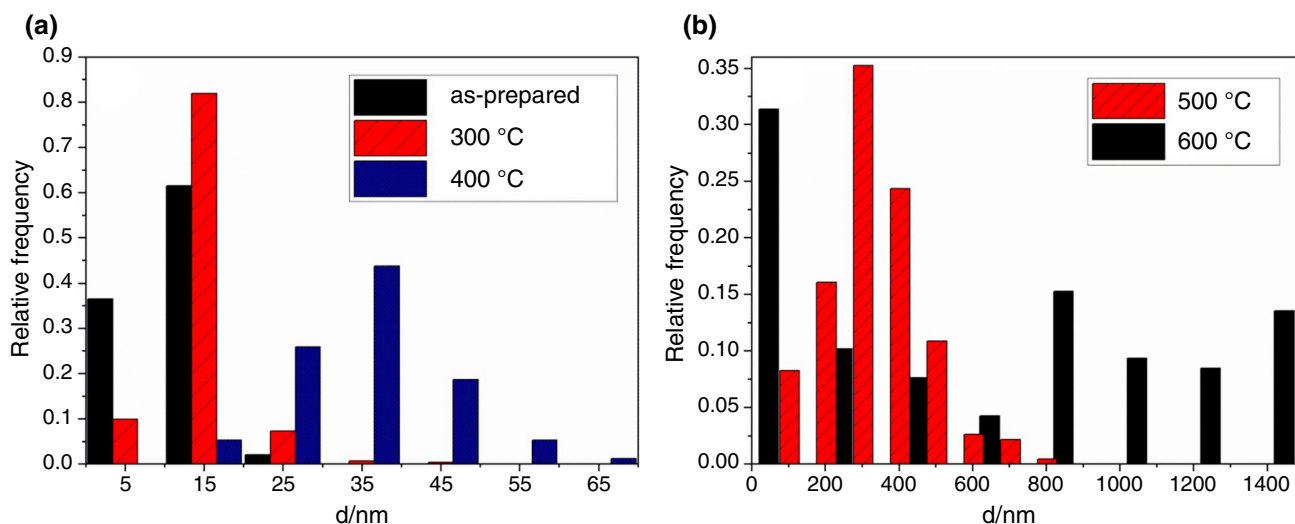


Fig. 2 Size distribution diagrams of **a** as-prepared sample and samples treated at 300 and 400 °C, and **b** samples treated at 500 and 600 °C (based on TEM images)

heat treatment temperature was increased, larger and larger particles formed, while the polydispersity of the system also increased. The as-prepared sample and the particles heat treated up to 400 °C show particle sizes generally below 50 nm, while after heat treatment at 500 and 600 °C the particle sizes drastically increased, reaching several hundreds of nm. It can be assumed that at these larger temperatures many particles aggregated to form much bigger particles: this caused an increasingly polydisperse system, especially after heat treatment at 600 °C, in which case the resulting system contained both very small and very large particles, even reaching the micrometre scale.

EDS analysis of the samples confirmed that the main component of the nanoparticles was LaF₃, and the presence of Yb and Er dopant was also observed in the EDS spectrum (see Supplementary Information for detailed EDS analysis results). EDS elemental mapping revealed (Fig. 1f) that after heat treatment at 600 °C, some of the particles had a different composition: most of the particles were made of LaF₃ with a small amount of Yb, but the main component in some

smaller particles was Yb instead of La. It was found that while the bigger particle that can be seen in Fig. 1f contains 0.25 mol% Yb and 0.18 mol% Er, the smaller particle contains 86.2 mol% Yb and 9.5 mol% Er. If we compare these values with the expected (according to stoichiometry) 5 mol% Yb and 0.5 mol% Er values, it can be concluded that at this high heat treatment temperature some of the doping Yb³⁺ and Er³⁺ ions left the LaF₃ crystals and segregated as new particles, and this resulted in their molar ratio decreasing in the remaining LaF₃ particles.

The average hydrodynamic diameters of the particles in ethanolic suspensions were determined by DLS and can be seen in Table 1. The hydrodynamic diameters are higher compared to the diameters determined by TEM, which is expected, since in ethanolic media the nanoparticles may form aggregates and the solvation shell also increases the measured size. This observation that the dispersion of nanoparticles in solution rarely leads to distribution at primary particle size has been shown for many other systems [20]. In Fig. 1a, a larger agglomerate of particles with a

size of ~200 nm can be observed—similar aggregates are likely present in ethanolic suspensions (or other liquid media). While the average hydrodynamic diameters are similar to each other in the case of the as-prepared sample and the sample treated at 300 °C, the value decreased after heat treatment at 400 °C, even though the particle size increased threefold according to TEM: it can be assumed that the increasing particle sizes and crystallinity resulted in decreased aggregation in this system. Furthermore, the diameter values significantly increase after heat treatment at 500 and 600 °C, due to the significantly increased nanoparticle sizes. Up until 400 °C, the polydispersity index remains a relatively low value, indicating a homogeneous dispersion with a relatively narrow size distribution. However, the samples treated at 500 and 600 °C show higher polydispersity index values, these dispersions are heterogeneous and the amounts of the fractions with different average sizes cannot be reliably determined.

Figure 3 shows the XRD patterns of the as-prepared and heat-treated samples. The samples all show peaks attributed to the hexagonal LaF_3 structure (PDF-00-032-0483). In the case of the as-prepared samples and the samples treated at 300 and 400 °C, all peaks correspond to this hexagonal crystal structure. The XRD pattern of the samples treated at 300 °C shows peaks with similar shape and intensity to the peaks of the as-prepared sample; however, after 400 °C the peaks become narrower with higher intensity, suggesting higher crystallinity. The sample treated at 400 °C still shows relatively wide peaks which can be attributed to a microcrystalline structure. At higher temperatures (500, 600 °C), the peaks become narrower, showing high crystallinity, and also

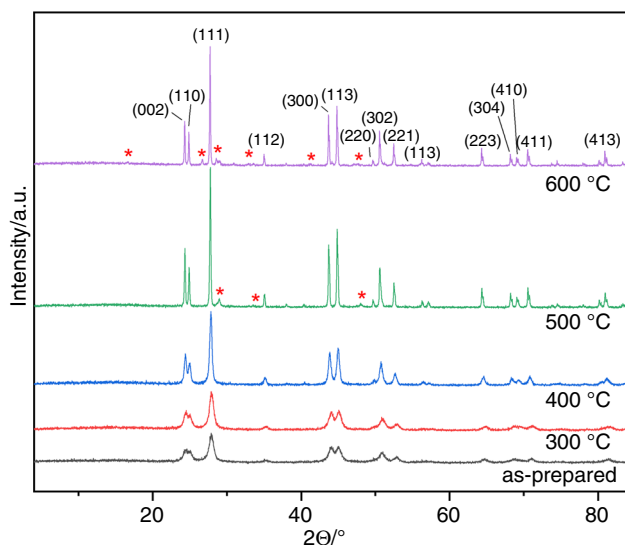


Fig. 3 XRD patterns of as-prepared and heat-treated samples; asterisk symbols show the new peaks appearing at 500 and 600 °C that do not belong to hexagonal LaF_3 structure

new smaller peaks appear, which means that a new crystal phase is present. This new phase is most likely due to one or more new by-products that are formed at higher temperatures during the heat treatment. This result is in accordance with the previously shown STEM EDS analysis, which indicates that the new crystal phase is made mainly of a compound of ytterbium. In the case of the sample treated at 500 °C, according to the peak positions, the new crystalline material is most likely YbOF (rhombohedral, PDF-04-021-9723). The analysis of the XRD pattern of the sample treated at 600 °C showed that this sample contains YbOOH (tetragonal, PDF-00-027-0964), and also possibly low amounts of graphite, which can originate from organic impurities. It can be assumed that during the heat treatment step, if the temperature is above 500 °C, some of the dopant ions leave the LaF_3 particles and form new crystalline phases, made of mainly YbOF, YbOOH and most likely other by-products which could not be detected. It can also be assumed, based on the STEM EDS, that the sample treated at 600 °C contains both YbOF and YbOOH particles, but only in small amounts, thus YbOF could no longer be identified by XRD. It also seems that erbium is a dopant in these new particles, partially replacing Yb in the crystal lattice.

In good accordance with the above observations, the calculated average crystallite sizes (Table 1) show that the 300 °C heat treatment was not enough to increase the crystallinity of the sample. However, from 400 °C, the increasing heat treatment temperature leads to increasing crystallite sizes. The sample treated at 600 °C showed by far the highest crystallite sizes. From Table 1, it can also be seen that while up to 400 °C the crystallite sizes are similar to the particle sizes determined by TEM, at higher temperatures the particle sizes are much higher compared to the determined crystallite sizes. This shows that at 500 and 600 °C the smaller crystals were more likely to aggregate and form much bigger particles.

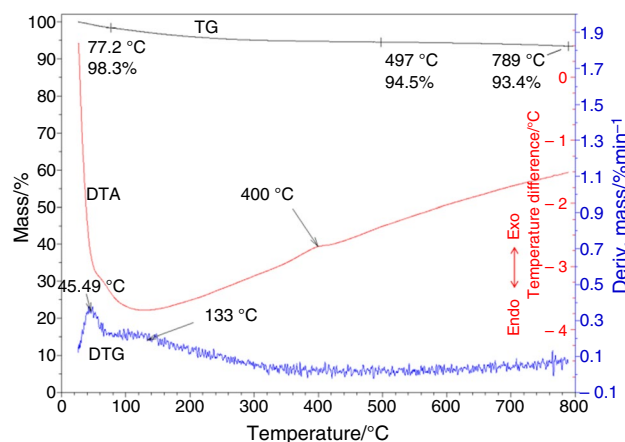


Fig. 4 TG/DTA analysis results of the as-prepared sample

TG/DTA analysis was carried out on the as-prepared sample, and the results can be seen in Fig. 4. The LaF_3 nanoparticles appear to be relatively stable and only undergo a small mass loss (6.6%) that can be attributed to the loss of water and small amounts of pollutants adsorbed on the surface of the particles, which is in good accordance with the literature [15, 21]. An exothermic heat effect can be observed on the DTA curve around 400 °C, which does not occur together with any mass loss, and which can be attributed to a crystallization process. This explanation is corroborated by the XRD results, which show increased crystallinity after heat treatment at 400 °C. Such a process of crystal structure adjustment was also shown in the literature by Shen et al. [15]; however, for their $\text{LaF}_3/20\% \text{Yb}, 5\% \text{Er}$ particles it was detected around 500 °C.

Characterization of upconversion properties

The green emission of all powder samples could be observed with the naked eye, under 980 nm excitation by a ~50 mW laser pointer (Roithner Lasertechnik, RLP-980-50F), with the exception of the as-prepared sample, which showed no emission. Upconversion emission was studied in detail by fluorescence spectroscopy measurements of ethanolic suspensions of the samples, using 980 nm excitation with laser power of 1.49 W. In all cases, three main emission peaks can be observed in the emission spectra of the samples (Fig. 5a): the highest intensity green emission peak is made of two smaller peaks at 521 and 540 nm, the peak with the next highest intensity is the red emission peak at 654 nm, and a small blue emission peak can also be observed at 408 nm. This is in good accordance with the literature, as Er^{3+} ion-doped upconverting materials

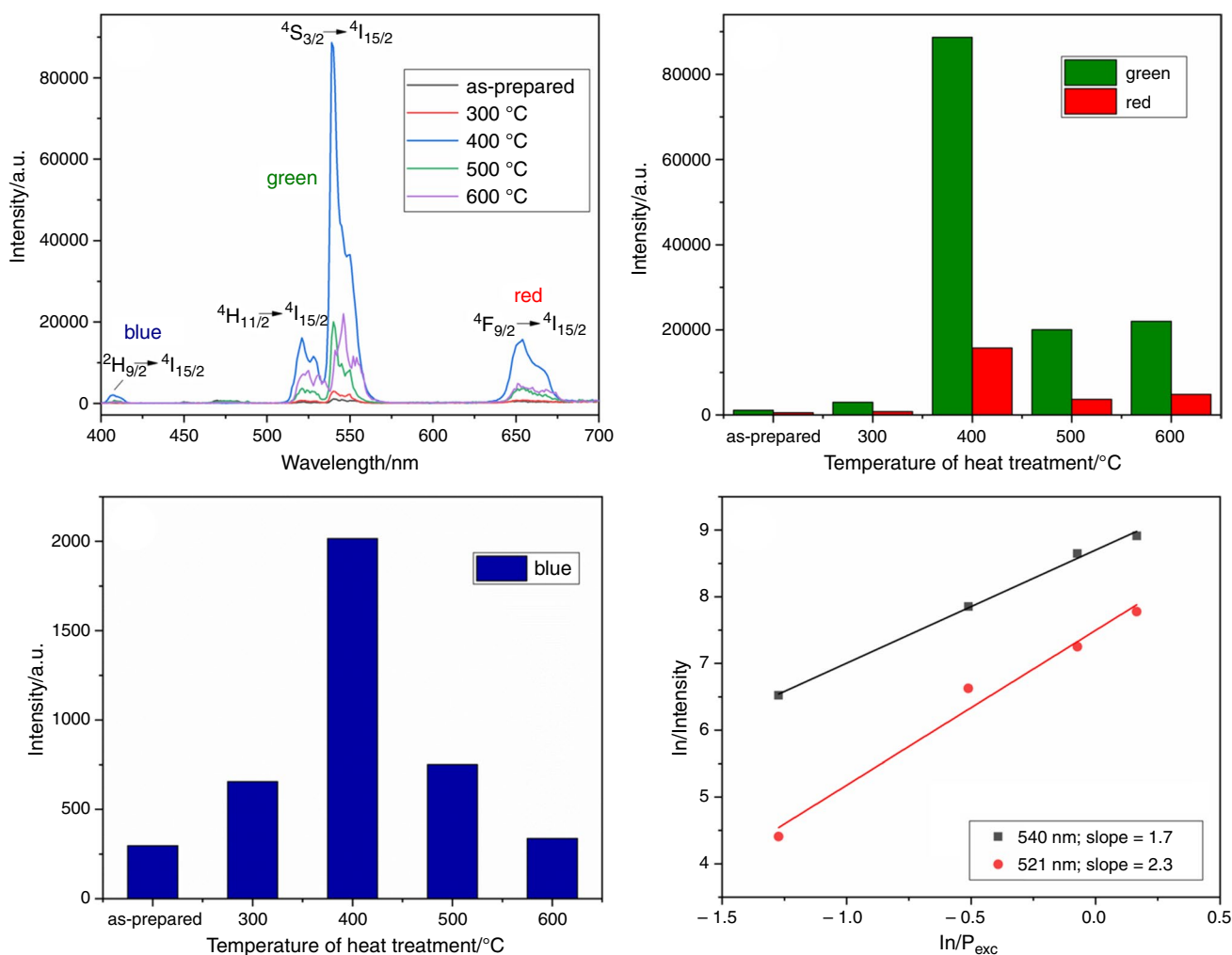


Fig. 5 a Upconversion emission spectra and b maximum intensity values of the green and red emission peaks and c blue emission peaks of the heat-treated UCNP samples; d logarithm of emission intensity

(at 521 and 540 nm) versus logarithm of laser power, measured on the sample treated at 400 °C

show similar emission spectra, and the peaks at 408, 521, 540 and 654 nm can be attributed to the $^2H_{9/2}$ to $^4I_{15/2}$, $^4H_{11/2}$ to $^4I_{15/2}$, $^4S_{3/2}$ to $^4I_{15/2}$ and $^4F_{9/2}$ to $^4I_{15/2}$ transitions of the Er^{3+} ion, respectively [15, 22].

Figure 5b shows the maximum intensity values of the green (540 nm) and red (654 nm) emission peaks of the samples treated at different temperatures, while Fig. 5c shows the values of the blue (408 nm) emission. It was true for all samples that the red and blue emission was significantly lower compared to the green emission. The sample heat treated at 400 °C showed by far the highest intensity emission for all peaks, which is an interesting result that differs from previous studies conducted on $LaF_3/Yb,Er$ particles with higher dopant concentrations [14–16], which did not report such a decrease in emission at higher temperatures. In the case of the green and red emission peaks, the samples with the next highest intensity are the samples treated at 600 °C and 500 °C, while the other samples show much lower intensity emission. In the case of the blue emission peak, the sample treated at 400 °C showed the highest intensity emission, followed by the samples treated at 500 °C and 300 °C.

Laser power-dependent emission intensity was also measured in the 500–600 nm emission wavelength range, to study the $^4H_{11/2}$ to $^4I_{15/2}$ (521 nm) and $^4S_{3/2}$ to $^4I_{15/2}$ (540 nm) transitions in the green emission peak: according to the literature [8, 22, 23], the logarithm of emission intensity depends linearly on the logarithm of the exciting laser power. Figure 5d shows this relation measured on the UCNPs samples treated at 400 °C. A line could be fitted to the data points: the slope of the fitted line can give information about how many photons are needed during excitation to produce the given emission peak [8, 22]. For both transitions, the slope value was close to 2, which means that two photons need to be absorbed in order for these emission peaks to appear in the spectra, which is in accordance with the determined transitions of the Er^{3+} ion [22].

Conclusions

UCNPs with relatively low rare earth ion doping (LaF_3 doped with 5 mol% Yb^{3+} and 0.5 mol% Er^{3+}) were synthesized and heat treated at different temperatures (300–600 °C), in order to investigate the role of heat treatment in the achieved properties, and especially the upconversion emission of the formed nanoparticles.

All prepared heat-treated nanoparticles showed upconversion properties (emission peaks, laser power-dependent behaviour) that are in accordance with results of Yb^{3+} - and Er^{3+} -doped upconverting materials described in the literature. The heat treatment temperature had an important effect on the upconversion emission of the particles, and

the highest intensity emission was achieved in the case of the sample heat treated at 400 °C. Based on the XRD and TG/DTA results, the main cause of the very low emission of the as-prepared sample and the sample treated at 300 °C is the lower crystallinity of these samples. However, as the heat treatment temperature was increased further, the emission intensity decreased, showing that high crystallinity was not the only important factor in reaching good upconversion emission. This is most likely due to the appearance of new crystal phases, as it was determined by the XRD measurement and the STEM EDS analysis: the Yb^{3+} and Er^{3+} dopant ions segregated and formed new particles ($YbOF$, $YbOOH$ crystals and other by-products), while their molar ratio decreased in the LaF_3 nanocrystals, which led to a significantly decreased upconversion emission intensity. Furthermore, the much higher particle sizes and broader size distribution that was observed after higher temperature heat treatments can also play a role in the decreased upconversion emission.

Supplementary Information The online version contains supplementary material available at <https://doi.org/10.1007/s10973-023-12417-5>.

Acknowledgements The authors thank András Szilágyi, László Seta and Adrien Paudics for their contributions to the research work and RCNS IMEC Functional Interfaces Research Group for DLS instrument use. This work was supported by the National Research Development and Innovation Office (K-128266). This research is part of projects no. TKP2021-NVA-02 and TKP2021-EGA-02, which have been implemented with the support provided by the Ministry of Culture and Innovation of Hungary from the National Research, Development and Innovation Fund, financed under the TKP2021-NVA and TKP2021-EGA funding scheme.

Authors' contribution Study conception and design were conducted by ZH, GT and BT. Material preparation, data collection and analysis were performed by GT and BT with contributions from the following people who conducted and interpreted different measurements: MK and DH for fluorimetry studies, GS for TEM and JM for XRD and TG/DTA analysis. The first draft of the manuscript was written by BT, and all authors commented on previous versions of the manuscript. All authors read and approved the final manuscript.

Funding Open access funding provided by Budapest University of Technology and Economics.

Declarations

Conflict of interest The authors have no competing interests to declare that are relevant to the content of this article.

Open Access This article is licensed under a Creative Commons Attribution 4.0 International License, which permits use, sharing, adaptation, distribution and reproduction in any medium or format, as long as you give appropriate credit to the original author(s) and the source, provide a link to the Creative Commons licence, and indicate if changes were made. The images or other third party material in this article are included in the article's Creative Commons licence, unless indicated otherwise in a credit line to the material. If material is not included in the article's Creative Commons licence and your intended use is not permitted by statutory regulation or exceeds the permitted use, you will

need to obtain permission directly from the copyright holder. To view a copy of this licence, visit <http://creativecommons.org/licenses/by/4.0/>.

References

- Gnach A, Bednarkiewicz A. Lanthanide-doped up-converting nanoparticles. *Nano Today*. 2012. <https://doi.org/10.1016/j.nantod.2012.10.006>.
- Pini F, Francés-Soriano L, Andriago V, Natile MM, Hildebrandt N. Optimizing upconversion nanoparticles for FRET biosensing. *ACS Nano*. 2022. <https://doi.org/10.1021/acsnano.2c12523>.
- Ansari AA, Sillanpää M. Advancement in upconversion nanoparticles based NIR-driven photocatalysts. *Renew Sustain Energy Rev*. 2021. <https://doi.org/10.1016/j.rser.2021.111631>.
- Kakavelakis G, Petridis K, Kymakis E. Recent advances in plasmonic metal and rare-earth-element upconversion nanoparticle doped perovskite solar cells. *J Mater Chem A*. 2017. <https://doi.org/10.1039/c7ta05428a>.
- Lin G, Jin D. Responsive sensors of upconversion nanoparticles. *ACS Sens*. 2021. <https://doi.org/10.1021/acssensors.1c02101>.
- Martínez ED, Brites CDS, Carlos LD, Urbano RR, Rettori C. Upconversion nanocomposite materials with designed thermal response for optoelectronic devices. *Front Chem*. 2019. <https://doi.org/10.3389/fchem.2019.00083>.
- Suo H, Zhu Q, Zhang X, Chen B, Chen J, Wang F. High-security anti-counterfeiting through upconversion luminescence. *Mater Today Phys*. 2021. <https://doi.org/10.1016/j.mtphys.2021.100520>.
- Haase M, Schäfer H. Upconverting nanoparticles. *Angew Chem Int Ed*. 2011. <https://doi.org/10.1002/anie.201005159>.
- Reddy KL, Balaji R, Kumar A, Krishnan V. Lanthanide doped near infrared active upconversion nanophosphors: fundamental concepts, synthesis strategies, and technological applications. *Small*. 2018. <https://doi.org/10.1002/sml.201801304>.
- Tek S, Vincent BK, Mimum LC, Tran AN, Shrestha B, Tang L, Nash KL. Lanthanum fluoride upconverting nanoparticles for photo-biomodulation of cell function. *Colloid Nanopart Biomed Appl XII*. 2017. <https://doi.org/10.1117/12.2253790>.
- Chang H, Xie J, Zhao B, Liu B, Xu S, Ren N, Xie X, Huang L, Huang W. Rare earth ion-doped upconversion nanocrystals: synthesis and surface modification. *Nanomaterials*. 2015. <https://doi.org/10.3390/nano5010001>.
- Kavand A, Serra CA, Blanck C, Lenertz M, Anton N, Vandamme TF, Mély Y, Przybilla F, Chan-Seng D. Controlled synthesis of NaYF₄:Yb Er upconversion nanocrystals as potential probe for bioimaging: a focus on heat treatment. *ACS Appl Nano Mater*. 2021. <https://doi.org/10.1021/acsnm.1c00664>.
- Laihinen T, Lastusaari M, Pihlgren L, Rodrigues LCV, Hölsä J. Thermal behaviour of the NaYF₄:Yb³⁺, R³⁺ materials. *J Therm Anal Calorim*. 2015. <https://doi.org/10.1007/s10973-015-4609-x>.
- Poma PY, Sales TO, Kumar KU, Jacinto C. Role of heat treatment on the structural and luminescence properties of Yb³⁺/Ln³⁺ (Ln=Tm, Ho and Er) co-doped LaF₃ nanoparticles. *Phys Chem Chem Phys*. 2020. <https://doi.org/10.1039/d0cp03316b>.
- Shen H, Wang F, Fan X, Wang M. Synthesis of LaF₃: Yb³⁺, Ln³⁺ nanoparticles with improved upconversion luminescence. *J Exp Nanosci*. 2007. <https://doi.org/10.1080/17458080701724943>.
- Acosta AL, Puga R, Loro H, Gómez KS. Synthesis of LaF₃ inorganic nanoparticles: Er³⁺, Yb³⁺ by the coprecipitation method and characterization by optical spectroscopy and electron microscopy. *J Phys Conf Ser*. 2018. <https://doi.org/10.1088/1742-6596/1143/1/012026>.
- Sevonkaev I, Matijević E. Formation of magnesium fluoride particles of different morphologies. *Langmuir*. 2009. <https://doi.org/10.1021/la901307t>.
- Lisjak D, Plohl O, Vidmar J, Majaron B, Ponikvar-Svet M. Dissolution mechanism of upconverting AYF₄:Yb, Tm (A = Na or K) nanoparticles in aqueous media. *Langmuir*. 2016. <https://doi.org/10.1021/acs.langmuir.6b02675>.
- Cullity BD. Elements of X-ray diffraction. London: Addison-Wesley; 1956.
- Murdock RC, Braydich-Stolle L, Schrand AM, Schlager JJ, Husain SM. Characterization of nanomaterial dispersion in solution prior to in vitro exposure using dynamic light scattering technique. *Toxicol Sci*. 2008. <https://doi.org/10.1093/toxsci/kfm240>.
- Hou X, He J, Yu L, Li Z, Zhang Z, Zhang P. Preparation and tribological properties of fluorosilane surface-modified lanthanum trifluoride nanoparticles as additive of fluoro silicone oil. *Appl Surf Sci*. 2014. <https://doi.org/10.1016/j.apsusc.2014.07.171>.
- De G, Qin W, Zhang J, Zhao D, Zhang J. Bright-green upconversion emission of hexagonal LaF₃: Yb³⁺, Er³⁺ nanocrystals. *Chem Lett*. 2005. <https://doi.org/10.1246/cl.2005.914>.
- Yan R, Li Y. Down/up conversion in Ln³⁺-doped YF₃ nanocrystals. *Adv Funct Mater*. 2005. <https://doi.org/10.1002/adfm.200305044>.

Publisher's Note Springer Nature remains neutral with regard to jurisdictional claims in published maps and institutional affiliations.